JOURNAL OF MATERIALS SCIENCE 27 (1992) 2053–2060

Relation between different inclusion–matrix interfaces in steels and the susceptibility to hydrogen embrittlement

E. SCHIAPPARELLI*, S. PRADO‡, J. J. TIEBAS*, J. GARIBALDI*
*Comisión Nacional de Energía Atómica, Dto. Materials, Av. del Libertador 8250, 1429 Buenos Aires, Argentina
‡Universidad Nac. de Trujillo, Apartado 530, Trujillo, Peru

The susceptibility to hydrogen damage of different steels with several heat treatments was studied in specimens hydrogenated during tensile testing. The initiation of localized cracking in hydrogenated specimens was dependent on the possibility of development of a critical hydrogen concentration, in the cavities and/or microcracks associated with undeformable inclusions such as Al_2O_3. The induction time to reach the critical hydrogen concentration depends on the hydrogen charging conditions, the matrix strength level and the undeformable inclusion content. The effect of the sulphur content in the steel and the MnS inclusion content is not important to the susceptibility of the steel to hydrogen damage.

1. Introduction

Several research works on hydrogen embrittlement (HE), considering the role played in this phenomenon by microstructural variables, have been reported [1–9]. None of the proposed mechanisms can adequately account for the effects of metallurgical variables, and detailed discussions referring to mechanisms are still likely to be premature. An essential step in understanding HE is to identify and understand the physical fracture processes which occur on the scale of the microstructure. According to Low [10], in general such processes can be divided into nucleation and propagation stages of the fracture events. In the case of ductile fracture the nucleation, growth and coalescence happen to be easier to understand, while other cases such as transgranular cleavage and intergranular fracture are rather less clearly known [11, 12]. Moreover in these latter cases there is even less understanding of how hydrogen alters or facilitates the various mechanisms.

In general it is accepted that strength level alone is not a reliable indicator of susceptibility to HE of low to medium strength level steels [13]. Results reported by Cain and Troiano [14] showed a broad scatter. In this work, the microstructure has been treated as a variable for steels of similar strength levels.

It should be emphasized that although there are a very large number of HE studies on record in which the microstructure of the material studied has been characterized superficially, particularly the inclusion content, the descriptions have not taken microstructural entities seriously enough, and the microstructure has rarely been altered in order to serve as an experimental variable.

Our experimental work has been focused on obtaining more complete and explicit information on the relation between matrix microstructure and inclusion content, and susceptibility to HE (SHE). In the studies on microstructure in steels, a non-conventional technique was used [15]. Particular attention has been paid to the influence of the different matrix–inclusion interface characteristics present in low, medium and high strength steels with regard to SHE.

2. Experimental procedure

2.1. Materials

Five steels in the form of plate were used for the study. The full chemical analyses are given in Table I. The microstructure of the steels was studied through optical microscopy (OM) and scanning electron microscopy (SEM).

Different heat treatments (HT) were given to the specimens; these are described in Table II. Heat treatments of the specimens were made in order to study the effects of the different microstructures and matrix–inclusions interfaces. The heat treatments were made in a furnace with a protective atmosphere to prevent oxidation.

2.2. Characterization of inclusions

The size, distribution, morphology, shape and number of the inclusions were studied by conventional light microscopy and scanning electron microscopy (Table III). An unconventional technique [15] was used to study the chemical composition of the phases that composed the inclusions. This is possible only if the inclusions are extracted from the matrix. With this technique, non-metallic inclusions in steel were extracted by means of an epoxy organic compound film. The steel surface was previously etched with

0022–2461

TABLE I Chemical composition of the steels (wt %)

	Material 1	Material 2	Material 3	Material 4	Material 5
C	0.27	0.18	0.92	0.33	0.186
S	0.016	0.003	0.04	0.009	0.017
P	0.014	0.01	0.03	0.014	0.013
Si	0.26	0.25	0.20	0.136	0.396
Mn	1.3	0.59	0.70	0.586	0.755
Al	0.019	0.017	0.015	0.018	0.028
Cr	–	0.89	–	1.56	13.8
Mo	0.29	0.21	–	0.409	0.041
Co	–	–	–	0.047	0.03
Ni	–	0.005	–	1.635	0.392
Sn	–	0.007	–	0.014	0.009
Cu	–	0.009	–	0.156	0.017
As	–	–	–	0.028	0.019
V	–	0.005	0.1	0.084	–
Ca	–	0.0031	0.002	–	–

TABLE II Different heat treatments

Material	Designation of HT type	Austenitizing treatment T(°C)	Heating time (min)	Coolant medium	Tempering temperature (°C)	Tempering time (min)
1	A_1	850	15	Oil	590	15
1	A_2	850	15	Oil	650	15
1	A_3	850	15	Oil	700	15
2	B_1	850	30	Air	–	–
2	B_2	850	30	Oil	–	–
2	B_3	850	30	Water	–	–
3	C_1	770	30	Water	–	–
3	C_2	770	30	Oil	200	15
3	C_3	770	30	Oil	400	30
4	D_1	850	30	Oil	–	–
4	D_2	850	30	Oil	400	30
5	F_1	1050	30	Water	–	–
5	F_2	1050	30	Oil	–	–
5	F_2	1050	30	Oil	650	30

HT: heat treatment.

TABLE III Inclusions content in steels

Material	Oxygen content in steel (p.p.m.)	Type A (undeformable particles)			Types B, C, D (deformable inclusions)		
		Size (μm)	Morphology	Chemical composition	Size (μm)	Morphology	Chemical composition
1	70	1–5	Spherical	SiO_2	1–5	Elongated	MnS
		1–5	Geometrical	Al_2O_3, SiO_2, Ca–aluminate			
2	72	1–7	Geometrical	Al_2O_3, Ca–aluminate	1–30	Elongated	Oxide–MnS
3	72	1–10	Geometrical	Al_2O_3, Ca–aluminate	1–45	Elongated	Oxide–MnS
4	30	1–4	Geometrical	Ca–aluminate	1–5	Elongated	Oxide–MnS
5	90	1–10	Geometrical	Al_2O_3	1–30	Elongated	Oxide–MnS

Br–CH_3OH solution, so that the inclusions were in relief, and it was then covered by an organic film. The inclusions were then extracted and the microstructure replicated. The conductivity of the sample was obtained by metallic deposition on the inclusions, and the phases that composed it were studied by energy-dispersive X-ray analysis (EDAX) associated with SEM. The same formalism as that used for thin foil was applied.

2.3. Hydrogen damage tests

Specimens were stressed in tension in a constant-load machine, as Fig. 1 shows schematically. In all cases the inclusions were oriented transverse to the tension direction. The specimens were charged galvanostatically in an electrochemical cell of acrylic material. A 0.1 N H_2SO_4 solution was used as electrolyte, with some traces of arsenite to facilitate hydrogen ingress into the metal. The current density was adjusted to

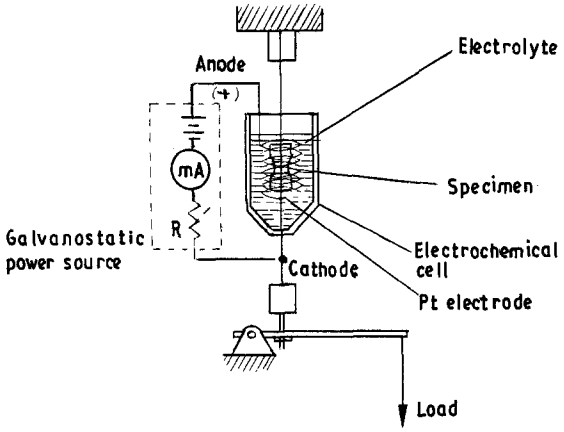

Figure 1 Scheme showing the electrochemical cell. The specimens were stressed in tension tests in a constant-load machine.

different values. The unexposed areas of the specimens were covered with an epoxy material.

2.4. Test specimens

The specimen geometry is shown in Fig. 2 and was developed by Blanco and Andreone [16].

3. Results

Some microstructures are shown in Figs 3 to 5. Some of the fracture surfaces are shown in Figs 6 to 10. The decohesion and/or cavities associated with hard inclusion–matrix interfaces after the hydrogen damage test, and the absence of decohesion in soft inclusion–matrix interfaces, is shown in Figs 11, 13 and 12, 14, respectively. The first observations were done in specimen zones marked ** in Fig. 2 that correspond to the yield zone. In zones next to the mark * in Fig. 2 that correspond to ultimate tensile strength crack propagation associated with hard particles, the appearance was as shown in Fig. 15.

The type of steel, matrix, hydrogen charge conditions, load applied, time for delayed fracture and fracture mode are shown in Table IV. The following comments are made on Table IV:

1. In general, when steel hardness and strength increase the SHE increases.

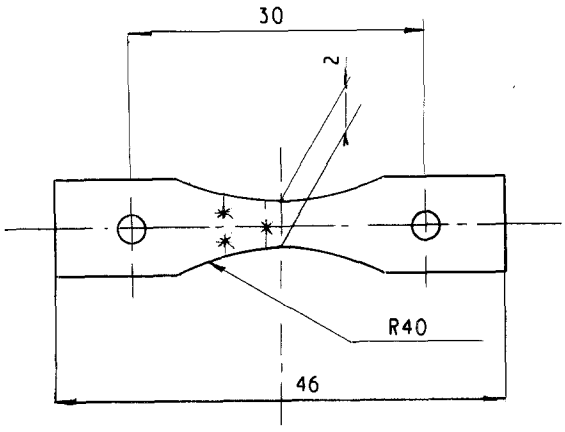

Figure 2 Scheme showing the specimen geometry and the observation zone: (**) yield strength, (*) ultimate tensile strength. Dimensions in mm.

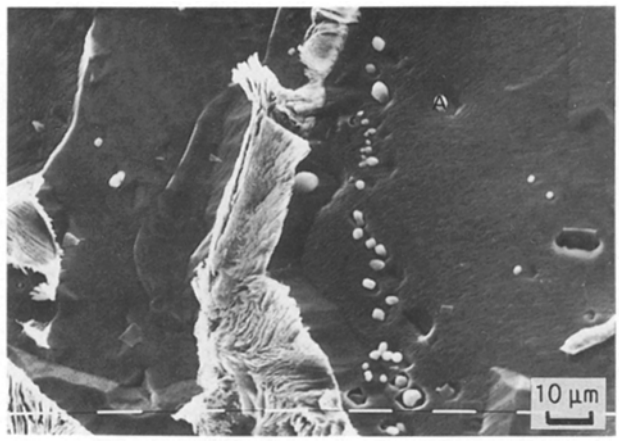

Figure 3 SEM microstructure of material 2 obtained by a non-conventional replica technique which allows a quantitative chemical analysis of the inclusion. A: cristobalite.

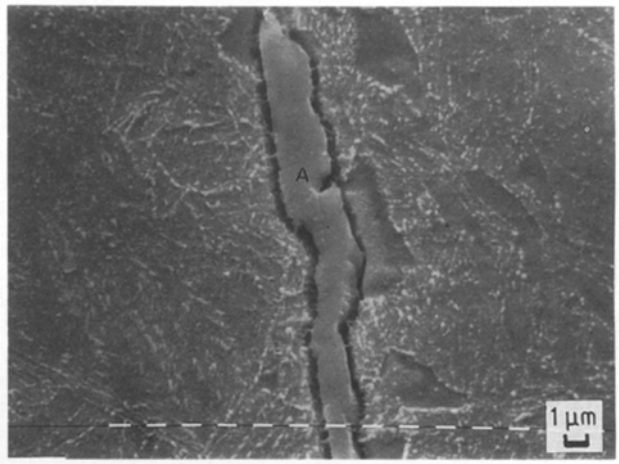

Figure 4 SEM micrograph showing the microstructure by a non-conventional replica technique of material 2. Tempered martensite matrix. A: MnS inclusion.

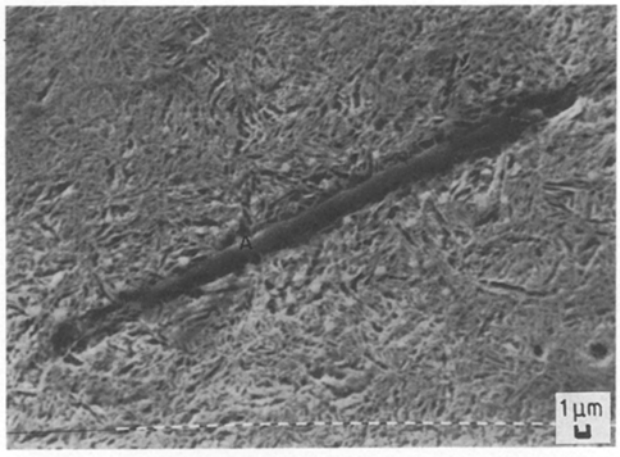

Figure 5 SEM micrograph showing the microstructure by a non-conventional replica technique of material 3. Tempered martensite matrix. A: rhodonite.

2. Notable differences are observed in fracture appearance and in the matrix type in those specimens with different SHE. These are summarized in Table V.

3. Looking at the results for specimens 31 to 34 in Table IV it is possible to observe the importance of the

TABLE IV SHE of several steels with different heat treatments

Specimen No.	Material	HT	Hardness (HV)	UTS (%)	Hydr.[a]	t_F (min)[b]	Fracture mode[c]	Current density (mA cm^{-2})	Type of matrix
1	1	A_1	356	93	Yes	2	C–I	10	Bain.
2	1	A_1	356	56	Yes	20	C–I	10	Bain.
3	1	A_1	356	37	Yes	50	C–I	10	Bain.
4	1	A_1	356	28	Yes	1500	C–I	10	Bain.
5	1	A_2	280	93	Yes	5	C–I	10	Ferr. per. bain.
6	1	A_2	280	65	Yes	20	C–I	10	Ferr. per. bain.
7	1	A_2	280	60	Yes	30	C–I	10	Ferr. per. bain.
8	1	A_3	260	93	Yes	100	D	10	Ferr. per.
9	1	A_3	260	84	Yes	1500	D	10	Ferr. per.
10	2	B_1	235	100	No	–	D	–	Ferr. per.
11	2	B_1	235	95	Yes	1600	D	20	Ferr. per.
12	2	B_2	393	100	Yes	–	D–C	–	Mart. bain.
13	2	B_2	393	32	Yes	7	D–I	20	Mart. bain.
14	2	B_2	393	18	Yes	5	D–I	20	Mart. bain.
15	2	B_2	393	17	Yes	4	D–I	20	Mart. bain.
16	2	B_3	420	100	No	–	D–C	–	Mart. bain.
17	2	B_3	420	23	Yes	35	I	20	Mart. bain.
18	2	B_3	420	21	Yes	14	I	20	Mart. bain.
19	3	C_1	813	100	No	–	C	–	Mart.
20	3	C_2	693	100	No	–	C	–	Mart.
21	3	C_3	495	100	No	–	C–D	–	Temper mart.
22	3	C_3	495	18	Yes	4	I	20	Temper mart.
23	3	C_3	495	22	Yes	7	I–D	20	Temper mart.
24	3	C_3	495	30	Yes	26	C–D	13	Temper mart.
25	3	C_3	495	34	Yes	35	C–D	12	Temper mart.
26	4	D_1	495	100	No	–	C–I	–	Temper mart.
27	4	D_1	495	0	Yes	0.5	I–C–D	20	Temper mart.
28	4	D_1	495	19	Yes	150	D–C–I	8.5	Temper mart.
29	4	D_1	495	100	No	–	C–I	–	Temper mart.
30	4	D_2	321	100	No	–	D–C	–	Bain. per.
31	4	D_2	321	24	Yes	9	I	20	Bain. per.
32	4	D_2	321	24	Yes	75	I–D	7	Bain. per.
33	4	D_2	321	30	Yes	52	D–I	3	Bain. per.
34	4	D_2	321	30	Yes	197	D–I	1.5	Bain. per.
35	5	F_1	558	100	No	–	C	–	Mart.
36	5	F_2	420	100	No	–	C	–	Bain.
37	5	F_2	420	5	Yes	6	I	20	Bain.
38	5	F_3	85	100	No	–	D	–	Ferr.
39	5	F_3	85	95	Yes	1600	C	20	Ferr.

[a] Load test with galvanostatic hydrogen charging.
[b] t_F is the induction time for delayed failure.
[c] C: cleavage, I: intergranular, D: ductile.

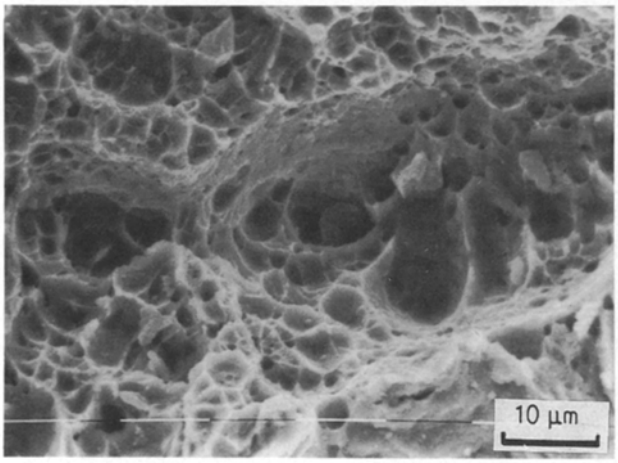

Figure 6 SEM micrograph showing the ductile fracture surface of material 2. Pearlite–ferrite matrix. Load test without galvanostatic hydrogen charging.

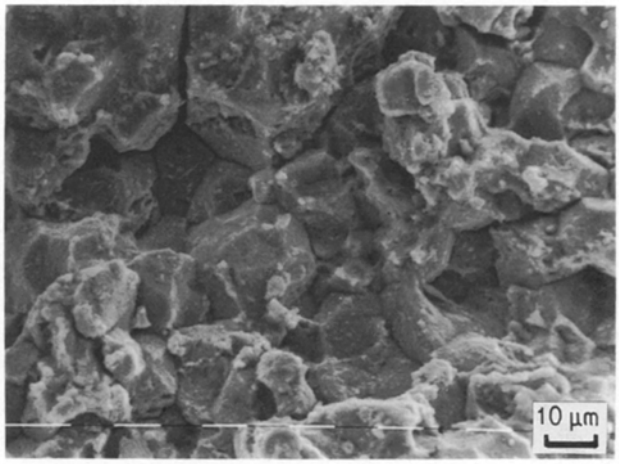

Figure 7 SEM micrograph showing the intergranular fracture surface of material 2. Martensite–bainite matrix. Corresponds to material in Fig. 4.

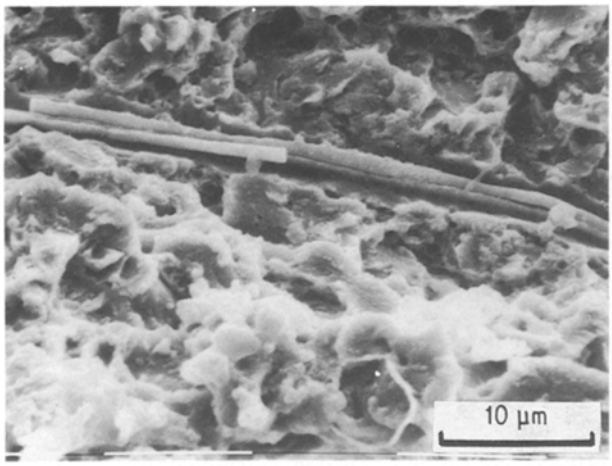

Figure 8 SEM micrograph showing the cleavage fracture surface of material 3. Martensite matrix. Corresponds to material in Fig. 5.

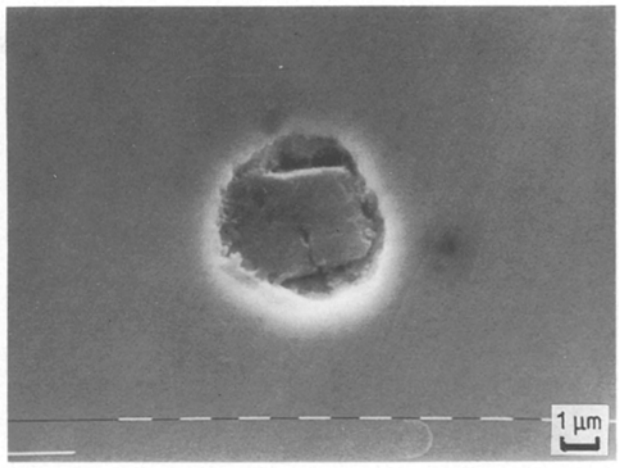

Figure 11 SEM micrograph showing hard inclusion–matrix decohesion. Material 2, martensite–bainite matrix. After hydrogen damage test. Observed zone in the specimen marked ** in Fig. 2.

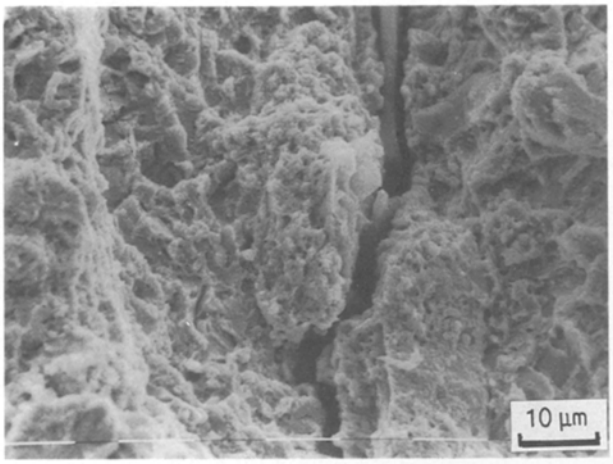

Figure 9 SEM micrograph of cleavage fracture surface of material 3. Tempered martensite matrix. Corresponds to Fig. 5. A secondary fissure is shown.

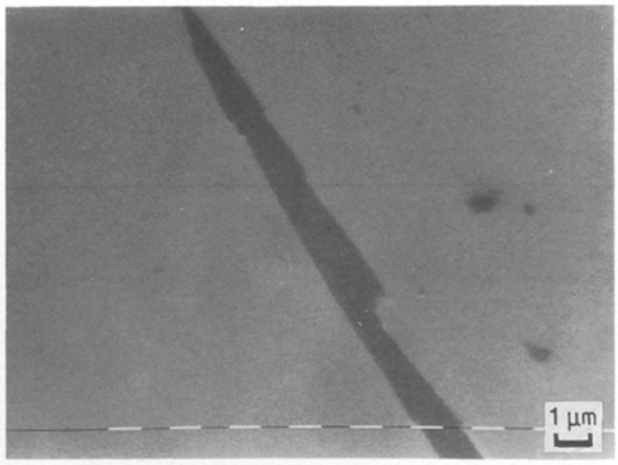

Figure 12 SEM micrograph showing no inclusion–matrix decohesion. Material 2, the same specimen as Fig. 11. The observed zone is * in Fig. 2.

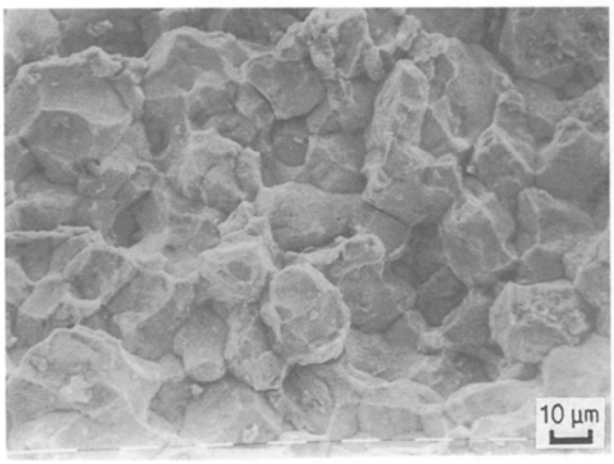

Figure 10 SEM micrograph showing the intergranular fracture surface of material 3. Tempered martensite matrix.

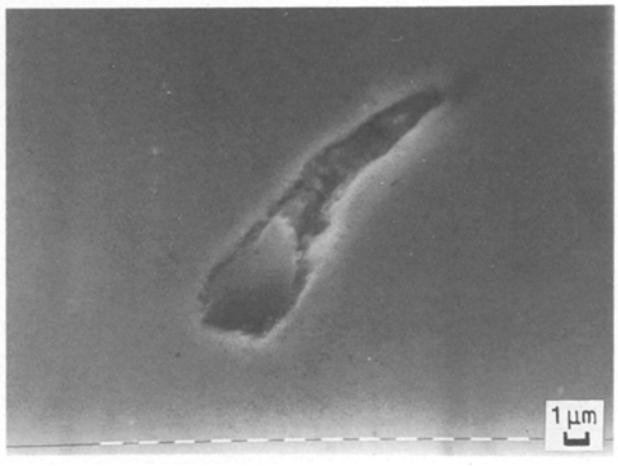

Figure 13 SEM micrograph showing hard inclusion–matrix decohesion. Material 3, tempered martensite matrix. After hydrogen damage test. Observed zone ** in Fig. 2.

current density value on the time period to produce fracture.

4. A very good reproducibility in the results was observed for each experiment. However, when different materials with similar resistance and/or hardness values are compared, the same correspondence between resistance and hardness against SHE is not found. We think this is associated with microstructural heterogeneities such as differences in hard inclusion content (e.g. specimen Nos 17 and 37).

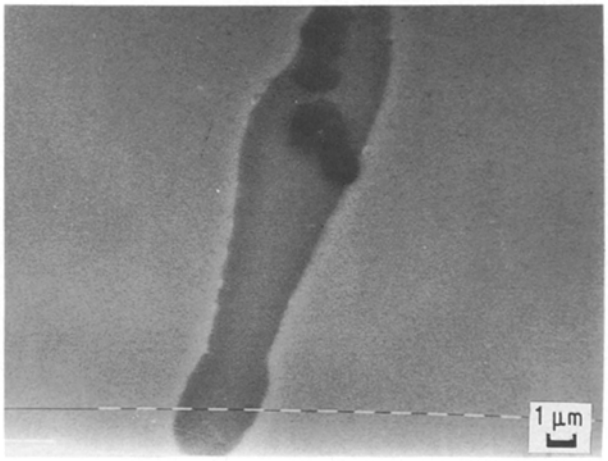

Figure 14 SEM micrograph showing no inclusion–matrix decohesion. Material 3, same specimen as Fig. 13. After hydrogen damage test. Observed zone * in Fig. 2.

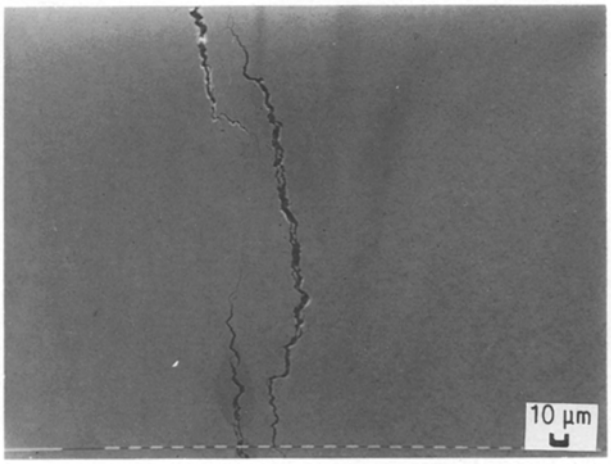

Figure 15 SEM micrograph of crack in material 3. Tempered martensite matrix. After hydrogen damage test. Observed zone * in Fig. 2. Inside the crack small particles of alumina are observed.

Crack initiation was studied by observation of the specimens by SEM as shown in Fig. 2. It was possible to determine approximately the load applied in each part of the specimen observed.

In all experiments with galvanostatic hydrogen-charged specimens, with the exception only of specimens that broke in a ductile manner, the generation of the microcracks associated with hard particle–matrix interfaces can be observed, even in the zone marked ** (yield strength zone), and fissures are seen in the zone marked * (next to the ultimate tensile strength zone). This can be observed in Figs 11, 13, 15 and 16. In the experiments without hydrogen charging, decohesion or cavity formation associated with hard particles was not observed in zones marked **. In experiments on specimens charged with hydrogen, cavities or cracks associated with plastically deformable particles such as MnS were not observed even in zones next to fracture; this is shown in Figs 12 and 14.

TABLE V Type of fracture appearance

SHE	Fracture mode	Type of matrix
High	Cleavage or intergranular	Martensitic Bainitic Martensitic–bainitic
Medium	Ductile–intergranular	Bainitic–pearlitic
Low	Ductile	Ferritic–pearlitic

4. Discussion

Pickering [17], Scheil and Schnell [18] and Malkiewicz and Rudnik [19, 20] have investigated the deformability of inclusions in steels. The characteristics of different inclusion–matrix interfaces present in steels, and their influence on the probability for the initiation of cavities and/or cracks during working processes of the steels, will be considered first. Secondly we shall try to explain our interpretation of how hydrogen induces crack initiation and makes crack growth possible.

There are different ways in which non-metallic inclusions can nucleate cracks in the steels. These depend on the relative plasticity of the inclusion phase and the steel phase. Only references to indigenous inclusions will be made, since it is well known that large exogenous inclusions in steel are likely to lead to the formation of cracks. The reason is that this inclusion type constitutes an area of weakness in the steel which may lead to crack formation and fracture, independent of the nature of the inclusion phase.

The nature of indigenous inclusions, their shape, size and distribution may be influenced in different ways. Taking into account the index of deformability (ν) developed by Malkiewikz and Rudnik [19] four cases may be considered:

Type A. Hard inclusions, with a relative plasticity (ν) of approximately zero, e.g. Al_2O_3 and Ca–Al_2O_3. During plastic deformation of the steel, an elongated ellipsoidal cavity is probably formed around these inclusions. When a neck is formed in the tensile specimen, non-longitudinal normal stresses increase the ellipsoidal cavity around the inclusion to propagate as a cleavage crack along the (0 0 1) cleavage planes. If the shape of the inclusion is not modified during deformation, it acts as a wedge which tends to force the cleavage planes apart.

Type B. Inclusions with an index of deformability $0 < \nu < 0.5$. The possibility that these particles act as wedges is smaller compared with hard inclusions. They do not introduce the same high stresses in possible cleavage planes.

Type C. Inclusions with an index of deformability $0.5 < \nu < 1$, for example MnS and silicates, are not expected to cause crack formation, because they act as stress raisers in the slip planes of the steels.

Type D. Inclusions with an index of deformability > 1 do not act as crack inducers in the parent steel phases.

Frequently the stress calculated in the usual manner (total load divided by the total cross-sectional area) is the nominal stress. This information is however of little value, if the actual working stress is not known due to stress raisers such as hard inclusions.

Stress raisers are generally not dangerous in ductile materials subjected to static loads. As the hardness

increases in materials, more sensitivity is produced to the effects of concentration of stress (by hard inclusions) under all loading conditions.

In previous observations [21–23] and in the present results, in all specimens charged with hydrogen under different conditions the only matrix–inclusion interfaces associated with hydrogen damage correspond to inclusions of type A, according to Table III. Similar observations were reported by Brooksbank and Andrews [24], Hewitt and Murray [25] and Cizewski [7].

The occurrence of the locations of crack initiation at hard inclusion–matrix interfaces is interpreted as follows: when the hydrogen is initially present within the metal it must be carried to zones of maximum stress [26, 27]. The conveyance of hydrogen can be made by normal lattice diffusion or by dislocation transport [28]. Once the hydrogen is available at the maximum stress location (matrix–hard particle interfaces type A), according to Table III a crack can potentially initiate there. This is understood as follows: the non-deformed inclusions are effective in concentrating the plastic deformation in steels [17–20]. It was reported by Bernard and Talbot [29] that hydrogen solubility in iron increases with strain level. It can be inferred that around hard inclusions, there is a higher hydrogen concentration in solid solution that could be in equilibrium with gaseous H_2 inside a cavity, and/or small cleavage cracks along the (0 0 1) cleavage plane in the matrix–inclusion interface. The aforementioned cavity could appear during steel working processes as described above. If the gaseous H_2 pressure in the cavity and/or microcracks is enough to produce a minimum critical shear stress in order to produce slip, then a critical nucleus size for cleavage will probably be produced. The study of the problem becomes difficult as the variation of the critical stress value with the stress and strain history of the metal must be taken into account.

4.1. Intergranular cracking by hydrogen

We must keep in mind that about 98% of all oxide inclusions are frequently smaller than 0.2 μm, although these small inclusions only represent about 1–2% of the total oxygen in the steel. If a great number of these inclusions appear at grain boundaries, the effect of the undeformable inclusions at grain boundaries with respect to the initiation of cracks could be the same, but an easier way to propagate the cracks will be the intergranular way. Intergranular cracking occurred in several experiments as shown in Table IV. The initiation of the crack at a grain boundary associated with an alumina particle can be seen in Fig. 16.

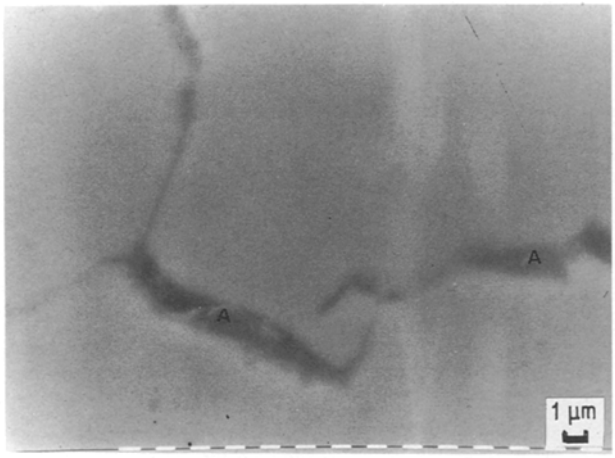

Figure 16 SEM micrograph of crack at grain boundary. Material 4. After hydrogen damage test zone. Observed zone ** in Fig. 2. A = alumina inclusion.

4.2. Significance of the effect of sulphur content on steel and the susceptibility to HE

According to extensive research [6, 8, 9], inclusions of MnS type are associated with hydrogen damage. A first suggestion as a guideline for steel selection is that for a given steel strength it is good to diminish the S level in the steel in order to reduce the MnS inclusion content. However, it should be taken into account that clean steels could have a high content of small alumina and Ca–aluminate inclusions, notwithstanding the oxygen content being frequently low. According to our previous and present observations these types of inclusion, hard particles, are those frequently associated with HE, according to the matrix strength and strain level of the steel, whereas MnS inclusions have a helpful effect as hydrogen sinks. In no case were cracks observed in the matrix–MnS inclusion interfaces. The induction time for delayed failure by hydrogen could be associated with hydrogen charge conditions, MnS quantity, and the characteristics of the hard particle–matrix interface, strength of the matrix and amount of plastic deformation of the steel during working processes.

5. Conclusions

For a constant value of strength of steel:

1. The susceptibility to hydrogen damage in steels depends on the characteristics of the matrix–inclusion interface. The nature, shape, size, localization and distribution of the inclusions have to be taken into account. Only interfaces of type A are associated with crack initiation. Interfaces of types B, C and D are never associated with crack initiation.
2. Only the undeformable inclusions are associated with hydrogen damage.
3. The S content and MnS inclusion content in steels do not influence the susceptibility of the steels to hydrogen damage.
4. The suggestion of lowering the S level in steel in order to diminish the MnS content is not important to improve the resistance to HE, but is very important to diminish the hard inclusion content.

Acknowledgements

The authors thank the Materials Department, and colleagues involved in this work. The generous assistance of the International Science Program, Uppsala University is gratefully acknowledged.

References

1. W. THOMPSON and I. BERNSTEIN, in "Advances in Corrosion Science and Technology", Vol. 7. edited by M. G. Fontana and R. Staehle (New York, 1980) p. 53.
2. Z. SZKLARSKA-SMIALOWSKA and E. LUNARSKA, *Werkst. Korros.* **32** (1981) 478.
3. I. BERNSTEIN and W. THOMPSON, *Int. Met. Rev.* **21** (1976) 87.
4. *Idem.*, in "Alloy and Microstructural Design", (edited by J. K. Tien and G. S. Ansell) (Academic, New York, 1976) p. 303.
5. D. WARREN, *Mater. Perf.* (January 1987) 38.
6. Y. KOBAYASHI and Z. SZKLARSKA-SMIALOWSKA, *Metall. Trans.* **17** (1986) 2255.
7. A. CIZEWSKI, in Conference Proceedings, "Stress Corrosion Cracking and Hydrogen Embrittlement of Iron Base Alloys", NACE-5, edited by R. Staehle, T. Hochmann, R. Cright and T. Slater, Houston, Texas (1977) p. 671.
8. G. PRESSOUYRE, R. BLONDEAU, G. PRIMON and L. GANDIOU, American Society for Metals, Metal Park, Ohio (1982) 212.
9. N. YOICHI, H. KURAHASHI, T. PMI and O. HIDA, *Trans. ISIJ* **19** (1979) 401.
10. J. LOW, *Progr. Mater. Sci.* **12** (1963) 1.
11. W. THOMPSON and I. BERNSTEIN, in "Fracture", Vol. 2, edited by D. M. Taplin (University of Waterloo Press, Waterloo, 1977) p. 249.
12. *Idem.*, in Proceedings, "Hydrogen in Metals", Paris, Vol. 10 (Pergamon, New York, 1977) paper 3A–6.
13. C. ZMUDZINSKI, L. BRETIN and N. TOITOT, *ibid.* Vol. 3, paper 6A–2.
14. W. CAIN and A. TROIANO, *Petrol. Engnr* **37** (1965) 78.
15. E. SCHIAPPARELLI, *Non-Destructive Testing Commun.* **3** (1987) 39.
16. E. BLANCO and C. ANDREONE, Doctoral thesis, CNEA (1984).
17. F. PICKERING, *JISI* **189** (1958) 148.
18. E. SCHEIL and R. S. SCHNELL, *Stahl. Eisen.* **72** (1952) 683.
19. T. MALKIEWICZ and S. RUDNIK, *JISI* **201** (1963) 33.
20. S. RUDNIK, *ibid.* **204** (1966) 374.
21. E. SCHIAPPARELLI and S. PRADO, in Proceedings of International Conference on Hydrogen Damage in Pressure Vessel Steels, Materials Properties Council, Paris, March 1989, in press.
22. E. SCHIAPPARELLI, *Mater. Perf.* (February 1988) 21.
23. *Idem., J. Mater. Sci.* **23** (1988) 3338.
24. D. BROOKSBANK and K. ANDREWS, "Production and Application of Clean Steels" (Iron and Steel Institute, London, 1972) p. 186.
25. I. HEWITT and I. MURRAY, *Br. Weld. J.* **15** (1968) 151.
26. J. LI, R. ORIANI and L. DARKEN, *Z. Phys. Chem.* **49** (1966) 271.
27. A. STEIGERWALD, W. SCHALLER and R. TROIANO, *Trans. Met. Soc. AIME* **218** (1960) 832.
28. J. TIEN, A. THOMPSON, I. BERNSTEIN and RICHARDS, *Met. Trans.* **7A** (1976) 821.
29. S. BERNARD and J. TALBOT, *Compt. Rend.* **244** (1957) 1193.

Received 9 November 1990
and accepted 26 July 1991